exposed to MWCNT promotes mesothelial cell proliferation *in vitro*.[30] Activated macrophages secrete a panel of growth factors and cytokines to regulate cell proliferation, which can augment transformation of mesothelial cells.[28,30,32,33] Our observations that mesothelial cell proliferation is enhanced by conditioned macrophage culture media and by the supernatants of pleural cavity lavage are consistent with these results, although the factors that are involved need to be identified.

Translocation of asbestos[34,35] and MWCNT[18] fibers from the lung to the pleural cavity has been found in rodents. This translocation also probably occurs in humans since asbestos fibers have been detected in human pleural lesions.[36] However, the mechanism and route of translocation are unclear. It has been suggested that penetration through the visceral pleura, possibly driven by increased pulmonary interstitial pressure and assisted by enhanced permeability of the visceral pleura due to asbestos-induced inflammation might be a major route.[37] In the present study, only a few MWCNT and CRO fibers were observed penetrating through the visceral pleura, and a large number of the fibers in the pleural cavity was observed in macrophages. We also observed frequent deposition of MWCNT and CRO in the mediastinal lymph nodes, mostly phagocytosed by macrophages. These results suggest that a probable route of translocation of the fibers is lymphatic flow. Inflammation in the pleural cavity is probably a defense response against translocated fibers. Murphy *et al.*[19] reported that intrapleural injection of 5 μg/mouse of long MWCNT or asbestos initiated sustained inflammation, including increased granulocyte number and protein level, in the pleural cavity. Thus, the observed proliferation of visceral mesothelial cells in the present study is probably caused by inflammatory reactions both in the lung and in the pleural cavity. In the present study, no MWCNT or crosidolite fibers or lesions were observed in the parietal pleura. This is possibly due to the short experimental period and limited amount of fibers in the pleural cavity, which would result in little inflammation in the parietal pleura.

Currently, the exposure level to MWCNT in the workplace is unknown and there are no administrational regulations for the occupational exposure limit for MWCNT. In November 2010, the National Institute of Occupational Safety and Health (NIOSH) released a non-official carbon nanotube exposure limit for peer review. The recommended exposure limit in the air was set at 7 μg/m^3.[38] Previously, we used a total dose of 1.25 mg/rat of titanium dioxide over a 9-day period and identified factors involved in titanium dioxide-induced lung lesions.[24] In the present study, we used the same protocol for the purpose of induction of observable pleural lesions and inflammation in the pleural cavity as well to ensure the presence of a detectable number of fibers in the pleural cavity after short-term administration; this dose was higher than the NIOSH exposure limit. Time- and dose-dependent experiments are needed in future studies, and further investigation is also required to elucidate cytokines and other factors that cause parietal mesothelial proliferation in animal models that are more relevant to humans.

The IPS/intratracheal instillation is a widely used method to evaluate the respiratory toxicity of particles. It should be noted that IPS/intratracheal instillation is a non-physiological method and possibly affects the migration and distribution of particles in the lung due to the pressure from spraying. However, IPS/intratracheal instillation is relevant for identifying factors to be examined using long-term, more physiologically relevant methods of CNT administration.

In summary, MWCNT and CRO fibers were found to translocate from the lung to the pleural cavity after intrapulmonary administration. Importantly, MWCNT and CRO treatment caused visceral mesothelial cell proliferation and inflammation in the pleural cavity. This mesothelial proliferation was plausibly induced by inflammatory events in the lung and pleural cavity and mediated primarily by macrophages. The similarity between MWCNT-N, MWCNT-M and CRO in translocation to the pleural cavity, induction of pleural cavity inflammation and induction of visceral pleural mesothelial proliferation suggests that MWCNT might cause asbestos-like pleural lesions.

Acknowledgments

This work was supported by Health and Labour Sciences Research Grants (Research on Risk of Chemical Substance 21340601) (grant numbers H19-kagaku-ippan-006, H22-kagaku-ippan-005).

Disclosure Statement

The authors have no conflict of interest.

References

1 Bonner JC. Nanoparticles as a potential cause of pleural and interstitial lung disease. *Proc Am Thorac Soc* 2010; **7**: 138–41.
2 Donaldson K, Murphy FA, Duffin R *et al.* Asbestos, carbon nanotubes and the pleural mesothelium: a review of the hypothesis regarding the role of long fibre retention in the parietal pleura, inflammation and mesothelioma. *Part Fibre Toxicol* 2010; **7**: 5.
3 Johnston HJ, Hutchison GR, Christensen FM *et al.* A critical review of the biological mechanisms underlying the *in vivo* and *in vitro* toxicity of carbon nanotubes: the contribution of physico-chemical characteristics. *Nanotoxicology* 2010; **4**: 207–46.
4 Nagai H, Toyokuni S. Biopersistent fiber-induced inflammation and carcinogenesis: lessons learned from asbestos toward safety of fibrous nanomaterials. *Arch Biochem Biophys* 2010; **502**: 1–7.
5 Pacurari M, Castranova V, Vallyathan V. Single- and multi-wall carbon nanotubes versus asbestos: are the carbon nanotubes a new health risk to humans? *J Toxicol Environ Health A* 2010; **73**: 378–95.
6 Tsuda H, Xu J, Sakai Y *et al.* Toxicology of engineered nanomaterials – a review of carcinogenic potential. *Asian Pac J Cancer Prev* 2009; **10**: 975–80.
7 Barrett JC. Cellular and molecular mechanisms of asbestos carcinogenicity: implications for biopersistence. *Environ Health Perspect* 1994; **102** (Suppl 5): 19–23.
8 Miller BG, Searl A, Davis JM *et al.* Influence of fibre length, dissolution and biopersistence on the production of mesothelioma in the rat peritoneal cavity. *Ann Occup Hyg* 1999; **43**: 155–66.
9 Okada F. Beyond foreign-body-induced carcinogenesis: impact of reactive oxygen species derived from inflammatory cells in tumorigenic conversion and tumor progression. *Int J Cancer* 2007; **121**: 2364–72.
10 Stanton MF, Wrench C. Mechanisms of mesothelioma induction with asbestos and fibrous glass. *J Natl Cancer Inst* 1972; **48**: 797–821.
11 Walker C, Everitt J, Barrett JC. Possible cellular and molecular mechanisms for asbestos carcinogenicity. *Am J Ind Med* 1992; **21**: 253–73.
12 Yang H, Testa JR, Carbone M. Mesothelioma epidemiology, carcinogenesis, and pathogenesis. *Curr Treat Options Oncol* 2008; **9**: 147–57.
13 Poland CA, Duffin R, Kinloch I *et al.* Carbon nanotubes introduced into the abdominal cavity of mice show asbestos-like pathogenicity in a pilot study. *Nat Nanotechnol* 2008; **3**: 423–8.
14 Sakamoto Y, Nakae D, Fukumori N *et al.* Induction of mesothelioma by a single intrascrotal administration of multi-wall carbon nanotube in intact male Fischer 344 rats. *J Toxicol Sci* 2009; **34**: 65–76.
15 Takagi A, Hirose A, Nishimura T *et al.* Induction of mesothelioma in p53+/− mouse by intraperitoneal application of multi-wall carbon nanotube. *J Toxicol Sci* 2008; **33**: 105–16.
16 Takagi A, Hirose A, Futakuchi M *et al.* Dose-dependent mesothelioma induction by intraperitoneal administration of multi-wall carbon nanotubes in p53 heterozygous mice. *Cancer Sci* 2012; **103**: 1440–4.
17 Ryman-Rasmussen JP, Cesta MF, Brody AR *et al.* Inhaled carbon nanotubes reach the subpleural tissue in mice. *Nat Nanotechnol* 2009; **4**: 747–51.
18 Mercer RR, Hubbs AF, Scabilloni JF *et al.* Distribution and persistence of pleural penetrations by multi-walled carbon nanotubes. *Part Fibre Toxicol* 2010; **7**: 28.
19 Murphy FA, Poland CA, Duffin R *et al.* Length-dependent retention of carbon nanotubes in the pleural space of mice initiates sustained inflammation and progressive fibrosis on the parietal pleura. *Am J Pathol* 2011; **178**: 2587–600.
20 Oka Y, Mitsui M, Kitahashi T *et al.* A reliable method for intratracheal instillation of materials to the entire lung in rats. *J Toxicol Pathol* 2006; **19**: 107–9.
21 Jackson P, Hougaard KS, Boisen AM *et al.* Pulmonary exposure to carbon black by inhalation or instillation in pregnant mice: effects on liver DNA strand breaks in dams and offspring. *Nanotoxicology* 2012; **6**: 486–500.
22 Morimoto Y, Hirohashi M, Ogami A *et al.* Pulmonary toxicity of well-dispersed multi-wall carbon nanotubes following inhalation and intratracheal instillation. *Nanotoxicology* 2012; **6**: 587–99.
23 Ogami A, Yamamoto K, Morimoto Y *et al.* Pathological features of rat lung following inhalation and intratracheal instillation of C(60) fullerene. *Inhal Toxicol* 2011; **23**: 407–16.
24 Xu J, Futakuchi M, Iigo M *et al.* Involvement of macrophage inflammatory protein 1alpha (MIP1alpha) in promotion of rat lung and mammary carcinogenic activity of nanoscale titanium dioxide particles administered by intrapulmonary spraying. *Carcinogenesis* 2010; **31**: 927–35.
25 Yanagihara K, Tsumuraya M, Takigahira M *et al.* An orthotopic implantation mouse model of human malignant pleural mesothelioma for *in vivo* photon counting analysis and evaluation of the effect of S-1 therapy. *Int J Cancer* 2010; **126**: 2835–46.
26 Adamson IY, Bakowska J, Bowden DH. Mesothelial cell proliferation after instillation of long or short asbestos fibers into mouse lung. *Am J Pathol* 1993; **142**: 1209–16.
27 Sekhon H, Wright J, Churg A. Effects of cigarette smoke and asbestos on airway, vascular and mesothelial cell proliferation. *Int J Exp Pathol* 1995; **76**: 411–8.
28 Adamson IY, Prieditis H, Young L. Lung mesothelial cell and fibroblast responses to pleural and alveolar macrophage supernatants and to lavage fluids from crocidolite-exposed rats. *Am J Respir Cell Mol Biol* 1997; **16**: 650–6.
29 Li XY, Lamb D, Donaldson K. Mesothelial cell injury caused by pleural leukocytes from rats treated with intratracheal instillation of crocidolite asbestos or *Corynebacterium parvum*. *Environ Res* 1994; **64**: 181–91.
30 Murphy FA, Schinwald A, Poland CA *et al.* The mechanism of pleural inflammation by long carbon nanotubes: interaction of long fibres with macrophages stimulates them to amplify pro-inflammatory responses in mesothelial cells. *Part Fibre Toxicol* 2012; **9**: 8.
31 Mutsaers SE, Whitaker D, Papadimitriou JM. Stimulation of mesothelial cell proliferation by exudate macrophages enhances serosal wound healing in a murine model. *Am J Pathol* 2002; **160**: 681–92.
32 Lechner JF, LaVeck MA, Gerwin BI *et al.* Differential responses to growth factors by normal human mesothelial cultures from individual donors. *J Cell Physiol* 1989; **139**: 295–300.
33 Wang Y, Faux SP, Hallden G *et al.* Interleukin-1beta and tumour necrosis factor-alpha promote the transformation of human immortalised mesothelial cells by erionite. *Int J Oncol* 2004; **25**: 173–8.
34 Choe N, Tanaka S, Xia W *et al.* Pleural macrophage recruitment and activation in asbestos-induced pleural injury. *Environ Health Perspect* 1997; **105** (Suppl 5): 1257–60.
35 Viallat JR, Raybuad F, Passarel M *et al.* Pleural migration of chrysotile fibers after intratracheal injection in rats. *Arch Environ Health* 1986; **41**: 282–6.
36 Kohyama N, Suzuki Y. Analysis of asbestos fibers in lung parenchyma, pleural plaques, and mesothelioma tissues of North American insulation workers. *Ann N Y Acad Sci* 1991; **643**: 27–52.
37 Miserocchi G, Sancini G, Mantegazza F *et al.* Translocation pathways for inhaled asbestos fibers. *Environ Health* 2008; **7**: 4.
38 NIOSH. Occupational exposure to carbon nanotubes and nanofibers. *Curr Intelligence Bull* 2010; **161-A**: 1–149.

Supporting Information

Additional Supporting Information may be found in the online version of this article:

Fig. S1. Characterization of multi-walled carbon nanotubes and crocidolite fibers in the suspensions.
Fig. S2. SEM observation of multi-walled carbon nanotubes and crocidolite fibers in the visceral pleura.
Fig. S3. Inflammation and fibrosis in the lung.
Fig. S4. Cytotoxicity of multi-walled carbon nanotubes and crocidolite to TCC-MESO1 cells *in vitro*.

doi: 10.1111/cas.12005

J Toxicol Pathol 2012; 25: 233–239

Original Article

Acute Phase Pulmonary Responses to a Single Intratracheal Spray Instillation of Magnetite (Fe_3O_4) Nanoparticles in Fischer 344 Rats

Yukie Tada[1]*, Norio Yano[1], Hiroshi Takahashi[1], Katsuhiro Yuzawa[1], Hiroshi Ando[1], Yoshikazu Kubo[1], Akemichi Nagasawa[1], Akio Ogata[1], and Dai Nakae[1,2]*

[1] Departments of Environmental Health and Toxicology, Tokyo Metropolitan Institute of Public Health, 3-24-1 Hyakunin-cho, Shinjuku-ku, Tokyo 169-0073, Japan
[2] Tokyo University of Agriculture, 1-1-1 Sakuragaoka, Setagaya-ku, Tokyo 156-8502, Japan

Abstract: Iron nanomaterials are of considerable interest for application to nanotechnology-related fields including environmental catalysis, biomedical imaging, drug delivery and hyperthermia, because of their superparamagnetic characteristics and high catalytic abilities. However, information about potential risks of iron nanomaterials is limited. The present study assessed pulmonary responses to a single intratracheal spray instillation of triiron tetraoxide nanoparticles (magnetite) in rats. Ten-week-old male and female Fischer 344 rats (n=5/group) were exposed to a single intratracheal spray instillation of 0 (vehicle), 5.0, 15.0 or 45.0 mg/kg body weight (BW) of magnetite. After 14 days, the rats were sacrificed, and biological consequences were investigated. The lung weights of the 15.0 and 45.0 mg/kg BW male and female groups were significantly higher than those of the control groups. The lungs of treated rats showed enlargement and black patches originating from the color of magnetite. The typical histopathological changes in the lungs of the treated rats included infiltration of macrophages phagocytosing magnetite, inflammatory cell infiltration, granuloma formation and an increase of goblet cells in the bronchial epithelium. The results clearly show that instilled magnetite causes foreign body inflammatory and granulating lesions in the lung. These pulmonary responses occur in a dose-dependent manner in association with the increase in lung weight. (DOI: 10.1293/tox.25.233; J Toxicol Pathol 2012; 25: 233–239)

Key words: magnetite, Fe_3O_4, nanoparticles, lung, intratracheal spray instillation, Fischer 344 rat

Introduction

Nanomaterials are defined as having a size of 100 nanometers or less in at least one dimension. Nanotechnology -the creation, manipulation and application of nanomaterials- involves the ability to engineer, control and exploit the unique chemical, physical and electrical properties that emerge from infinitesimally tiny man-made particles[1]. Engineered nanoparticles, the surface volume increases, can result in having unique photonic and catalytic properties that display great differences from those of over-nanoscaled materials with the same composition. The superb biological and environmental reactivities of nanoparticles have led to their wide and considerable use in disease treatment, pollutant degradation and so forth[1, 2]. Among them, iron nanomaterials are of considerable interest for application to nanotechnology-related fields including environmental catalysis, magnetic storage, biomedical imaging[1], magnetic target drug delivery[3, 4] and hyperthermia[5–8] because of their superparamagnetic characteristics and high catalytic abilities.

Acute toxic reactions of nano-magnetic ferrofluid have been evaluated, and half lethal doses (LD_{50}) of >2104.8, >438.50 and >1578.6 mg/kg were found in cases of oral, intravenous and intraperitoneal administrations, respectively, where no apparent pathological changes were observed[9]. It was shown *in vitro* that triiron tetraoxide, Fe_3O_4, causes a decrease in mitochondrial function and lactate dehydrogenase leakage in Neuro-2A cells only with concentrations reaching greater than 200 μg/mL[10]. Magnetic nanoparticles of Fe_3O_4 affect the ICR mice immune system such that Fe_3O_4 nanoparticles enhance the production of interleukin (IL)-2, interferon-γ and IL-10, but not IL-4, in the peripheral blood[11]. A high amount of magnetite, 15 mg × 15 intratracheal instillations, led to an unexpected lung tumor in the female Wistar rat[12], while chronic exposure to iron oxide has been shown not to increase the incidence of pulmonary tumors[13, 14]. Iron is a transition metal that is considered to play a pivotal role in modulating oxidative stress and other biological responses[15, 16], which is speculated to be the critical mechanism in eliciting the adverse effects of iron particulate matter exposure. Despite the above information, the risk data for iron nanomaterials are limited. The present study assessed pulmonary responses to a single intratracheal spray instillation of Fe_3O_4 nanoparticles (magnetite) in male and female Fischer 344 rats.

Received: 12 March 2012 , Accepted: 19 June 2012
*Corresponding authors: Y Tada (e-mail: Yukie_Tada@member.metro.tokyo.jp), D Nakae (e-mail: agalennde.dai@nifty.com)

Materials and Methods

Ethical considerations

The current study was performed principally in conformity with the Guidelines for the Toxicity Testing of Pharmaceuticals released by the MHLW (Ministry of Health, Labour and Welfare) of Japan (http://www.pmda.go.jp/ich/s/s4_93_8_10.pdf). The experimental protocol was approved by the Experiments Regulation Committee and Animal Experiment Committee of the Tokyo Metropolitan Institute of Public Health prior to its execution. All the animals were handled in accordance with the Japanese Government Animal Protection and Management Law, Japanese Government Notification on Feeding and Safekeeping of Animals and the Guidelines for Animal Experimentation issued by the Japanese Association for Laboratory Animal Science[17].

Animals

A total of 42 male and female specific pathogen-free Fischer 344 (F344/DuCrlCrlj) rats were purchased at 8 weeks of age from Charles River Laboratories Japan, Inc. (Kanagawa, Japan). The rats were housed individually in stainless steel cages and were kept under controlled conditions of temperature (22–24°C), relative humidity (50–60%) and ventilation (more than 10 times/hour) with a 12-hour light/dark cycle; they were allowed free access to pelleted chow CE-2 (CLEA Japan, Inc., Tokyo, Japan) and drinking water throughout both the acclimation and experimental periods. After confirming normal health status at the end of the 2-week acclimation period, 20 rats of each sex were selected for use and randomly allocated to 4 groups of 5 rats. The rats were observed twice daily, and clinical signs and mortality were recorded.

Test chemical and animal treatments

The magnetite slurry (Fe_3O_4 nanoparticle suspension; lot number, 90828) was generously supplied by Toda Kogyo Corp. (Otake, Hiroshima, Japan). A representative transmission electron microscopic (TEM) view of magnetite particles is shown in Fig. 1. The estimated primary particle size of the prepared sample is 5–15 nm in diameter (TEM measurement). The purity of the test chemical was determined by an energy dispersive X-ray spectrometer, and only iron and oxygen were detected. Prior to the toxicity study, the optimal way to disperse magnetite was preliminarily examined. Magnetite was dispersed in physiological saline, physiological saline+0.05% tween 80, 0.1 M Tris buffer (pH 8.0), 0.5% carboxymethyl cellulose, 0.1 M phosphate buffer (pH 8.1) or ultrapure water (Milli-Q water, 18.2 MΩ). Observation of dispersed particles was carried out under a light microscope and judged on the basis of Brownian motion. Among these test dispersion vehicles, Milli-Q water was the best vehicle to obtain the most homogeneous suspension. Magnetite slurry was thus diluted with sterile Milli-Q water and adjusted to about pH 7.4 with 0.1 N hydrochloric acid. The intratracheal instillation technique was performed according to the recommendations of Driscoll *et al.*[18]. Before the intratracheal spray instillation, the rats were anesthetized by diethyl ether and placed in a supine position on an angled board with their necks extended. Magnetite suspension was placed in an ultrasonication bath (SONOREX RK31, BANDELIN electronic, Berlin, Germany) and then instilled into the trachea by a sterile stainless steel tube (IA-1B Micro-Sprayer, Penn-Century, Inc., Wyndmoor, PA, USA) at the concentrations of 0 (control), 5.0 (low), 15.0 (middle) and 45.0 (high) mg/1 mL/kg body weight, which was followed by the insufflation of 0.2 mL of air.

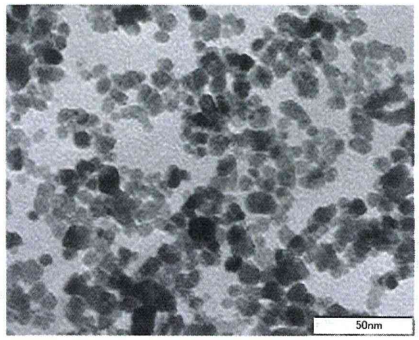

Fig. 1. Representative transmission electron microscopic view of magnetite nanoparticles. The estimated primary particle size is about 5–15 nm in diameter.

Animal sacrifice and assessments

Two weeks after instillation, all rats were deprived of food (but not water) overnight. The rats were then lightly anesthetized by diethyl ether and sacrificed by exsanguination after collecting blood samples via the abdominal aorta. The blood for hematology was collected into tubes treated with dipotassium ethylenediaminetetraacetate (EDTA-2K). The hematological examination was carried out using an automatic analyzer (Sysmex KX-21NV; Sysmex Corporation, Kobe, Hyogo, Japan) to determine the red blood cell count (RBC), hemoglobin concentration (HGB), hematocrit level (HCT), mean corpuscular volume (MCV), mean corpuscular hemoglobin (MCH), mean corpuscular hemoglobin concentration (MCHC), white blood cell count (WBC) and platelet count (PLT). Differential counts of leukocytes were made by a light microscopic observation of smeared specimens stained with a routine May-Grünwald-Giemsa protocol. A serum biochemistry analysis was performed with an automatic analyzer (TBA-120FR; Toshiba Medical Systems

Table 1. Initial and Final Body Weights and Lung Weights in Fischer 344 Rats Treated with a Single Intratracheal Administration of Magnetite on Day 14

Item	Dose of magnetite (mg/kg body weight)			
	0 (control)	5.0	15.0	45.0
Males				
Initial number of rats	5	5	5	5
Initial body weight (g)	213.6 ± 3.9[a]	211.7 ± 5.5	214.9 ± 4.6	212.9 ± 4.0
Final effective number of rats	5	5	5	5
Final body weight (g)	239.4 ± 8.6	239.1 ± 7.4	239.1 ± 10.3	229.0 ± 2.8
Absolute lung weight (mg)	722.4 ± 27.4	823.8 ± 58.0	923.4 ± 91.5*	1105.1 ± 94.5*
Relative lung weight (mg/100 g BW)	301.9 ± 9.5	344.4 ± 19.4	386.4 ± 38.1*	482.5 ± 41.0*
Females				
Number of rats	5	5	5	5
Initial body weight (g)	138.9 ± 7.1	138.0 ± 5.8	138.6 ± 7.7	141.8 ± 9.3
Final effective number of rats	5	5	4	4
Final body weight (g)	151.0 ± 6.7	148.7 ± 6.1	149.3 ± 6.6	145.2 ± 12.4
Absolute lung weight (mg)	556.7 ± 77.2	642.1 ± 55.5	724.9 ± 88.1*	821.7 ± 68.0*
Relative lung weight (mg/100 g BW)	368.3 ± 46.6	431.3 ± 23.5	485.6 ± 57.7*	566.7 ± 32.6*

[a] Values are means ± standard deviations. *Significantly different from the corresponding control values ($P<0.05$, Dunnet's test).

Corporation, Tokyo, Japan) to determine the levels of total protein (TP), albumin (ALB), albumin/globulin ratio (A/G), glucose (GLU), aspartate aminotransferase (AST), alanine aminotransferase (ALT), total cholesterol (T-CHO), triglyceride (TG), total bilirubin (T-BIL), blood urea nitrogen (BUN), creatinine (CRE) and uric acid (UA). Upon sacrifice, the rats were macroscopically examined and subjected to a full autopsy. The brain, heart, lung (including bronchi, fixed by inflation with fixative), spleen, liver, kidneys, testes and ovaries were weighed and then fixed in 10% neutrally buffered formalin. Paraffin-embedded sections were routinely prepared and histopathologically examined after being stained with hematoxylin and eosin (HE), Azan Mallory and Berlin blue procedures.

Statistical analysis

For numerical data such as body and organ weights and hematological and serological outcomes, equality of means between the values of the control group and those of each treated group was assessed by Bartlett's test. Homogeneity of variance was then analyzed by one-way analysis of variance, and finally, differences between the values of the control group and those of each treated group were evaluated by Dunnett's test. If the Bartlett's test was significant, the data were subjected to the Kruskal-Wallis test and Dunnett's-type rank sum test. For contingent data such as incidences of histopathological lesions, differences between the values of the control group and those of each treated group were evaluated by Fisher's exact probability test[19]. Statistical processing was conducted using the StatLight software (Yukms Co., Ltd., Tokyo, Japan). Intergroup differences were considered statistically significant when P-values less than 0.05 were obtained.

Results

General findings

All male rats survived throughout the experimental period. In the females, one rat in each of the middle- and high-dose groups died within 1 hour from deep anesthesia following intratracheal spray instillation. After instillation, the male and female rats in the high-dose group were slightly less active than the control rats but recovered later.

Hematology and serum biochemistry

In the hematology, the HGB of the high-dose group males was significantly but slightly higher than that of the male control group. In the serum biochemistry, the A/G of the high-dose group females was significantly lower than that of the female control group. There were no significant differences in other items of hematology or biochemistry between the control and treated rats at any doses. Morphological findings and differential counts of leukocytes showed no significant effects in any of the treated groups.

Pathology

There were no significant differences in the initial or final body weights between the control and treated groups of either sex. Absolute and relative lung weights of the treated groups were higher than those of the control groups, and the differences were statistically significant for the middle- and high-dose groups (Table 1). In the male rats, the absolute and relative testes weights of the low-dose group were significantly higher than those of the control group. There were no significant differences in other organ weights between the control and treated groups for both sexes.

At necropsy, the lungs of the magnetite-treated groups of both sexes were enlarged, and scattered dark brown patches were observed in almost every lobe in all treated rats (Fig. 2). These changes were more marked in the middle- and high-dose groups than in the low-dose groups.

Fig. 2. Representative gross views of cross-sections of the formalin-fixed lungs from Fischer 344 rats treated with a single intratracheal spray instillation dose of 0 (control, A), 5.0 (B), 15.0 (C) or 45.0 (D) mg/kg body weight of magnetite on day 14. The enlargement and a large number of scattered dark brown patches are marked in almost every lobe at the middle and high doses.

Table 2. Histological Findings of the Lungs and Parathymic Lymph Nodes in Fischer 344 Rats Treated with a Single Intratracheal Administration of Magnetite on Day 14

Item	Dose of magnetite (mg/kg body weight)			
	0 (control)	5.0	15.0	45.0
Males				
Effective number of rats	5	5	5	5
Lung				
Inflammatory cell infiltration	0[a]	4*	4*	5*
Infiltration of macrophages phagocytosing magnetite	0	5*	5*	5*
Granuloma	0	1	3	5*
Increase of goblet cells in the bronchial epithelium	0	0	0	5*
Parathymic lymph nodes				
Infiltration of macrophages phagocytosing magnetite	0	5*	5*	5*
Deposit of magnetite	0	5*	5*	5*
Females				
Effective number of rats	5	5	4	4
Lung				
Inflammatory cell infiltration	0	3	4*	4*
Infiltration of macrophages phagocytosing magnetite	0	5*	4*	4*
Granuloma	0	0	1	4*
Increase of goblet cells in the bronchial epithelium	0	0	0	3
Parathymic lymph nodes				
Infiltration of macrophages phagocytosing magnetite	0	5*	4*	4*
Deposit of magnetite	0	5*	4*	4*

[a] Number of rats with the lesion. *Significantly different from the corresponding control values ($P<0.05$, Fisher's exact test). No apparent histological changes were observed in the other organs, when compared with the control rats.

Additionally, dark brown patches were also observed in the parathymic lymph nodes of male and female rats in all treated groups.

The histopathological changes in the lungs and parathymic lymph nodes are summarized in Table 2. In the lungs of most of the rats in all the treated groups, typically observed changes included the infiltration of multinucleated cells and lymphocytes (Fig. 3A) and the infiltration of dark-brownishly pigmented macrophages phagocytosing magnetite in the alveolar walls and spaces (Fig. 3B). In addition, granulomas were observed in 1, 3 and 5 of the low-, middle- and high-dose males and in 1 and 4 of the middle- and high-dose females, respectively. The granulomas were characterized by the aggregation of macrophages phagocytosing magnetite, inflammatory cell infiltration and proliferation of collagenous fiber (Fig. 3C and D). Reactive changes in alveolar and bronchial epithelia were observed in most of the rats of all treated groups and in the high-dose groups, respectively. An increase of goblet cells in the bronchial epithelium was observed in 5 and 3 of the high-dose males and females, respectively (Fig. 4). In the parathymic lymph nodes, infiltration of macrophages phagocytosing magnetite and deposits of magnetite particles were observed in male and female rats of all treated groups (Fig. 5). Dark-brownishly pigmented macrophages were observed at the center or end of the lymph node. No treatment-related changes were observed in other organs of either sex, whereas sporadic spontaneous lesions were observed identically in the control and treated rats.

Discussion

In the present study, rats were exposed to the magnetite nanoparticles by a single intratracheal spray instillation

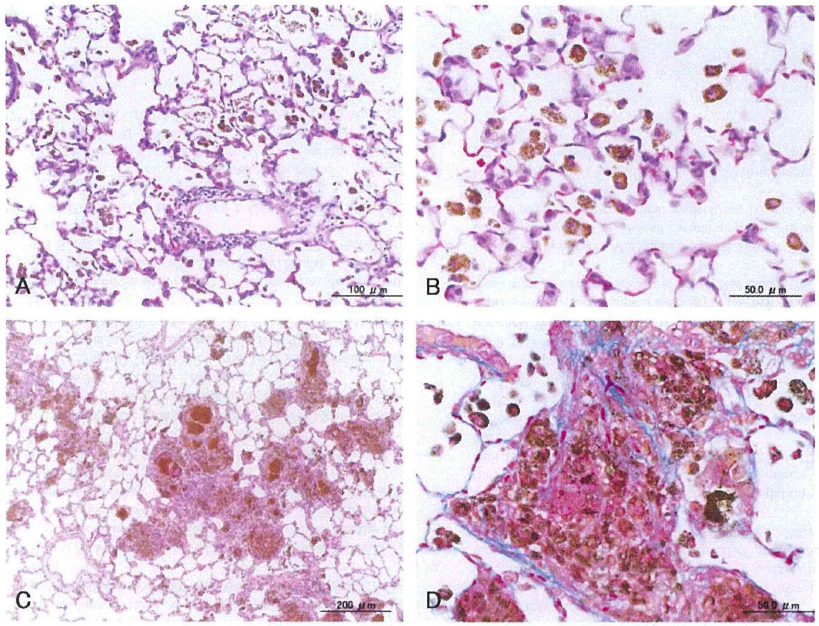

Fig. 3. Representative histologies of the lungs from Fischer 344 rats treated with a single intratracheal spray instillation dose of 5.0 (A, B) or 45.0 (C, D) mg/kg body weight of magnetite on day 14 (A–C, hematoxylin and eosin; D, Azan-Mallory). Infiltration of inflammatory cells (A) and alveolar macrophages phagocytosing magnetite particles (B) are evident in rats given the low dose. Granulomas consisting of macrophages with magnetite particles, infiltrating inflammatory cells and proliferative collagenous fiber (C and D) are evident in rats given the high dose.

Fig. 4. Representative histology of the lung from Fischer 344 rat treated with a single intratracheal spray instillation dose of 45.0 mg/kg body weight of magnetite on day 14 (hematoxylin and eosin). An increase in goblet cells in the bronchial epithelium is evident in a rat given the high dose.

at the doses of 0, 5.0, 15.0 and 45.0 mg/kg body weight. Macroscopically, enlargement of the lung was marked at middle and high doses. Black patches were scattered in almost every lobe of the lungs and the lung-associated lymph nodes of all treated rats. Two weeks after instillation, a large amount of the administered magnetite remained in the lung, and some of the magnetite was distributed into the regional lymph nodes. Histopathologically, infiltration of macrophages phagocytosing magnetite, multinucleated cells and lymphocytes were observed in the lungs of the treated rats. In addition, granulomas were observed in the lungs of the treated rats. Infiltration of multinucleated cells and lymphocytes which supposed to be macrophages, generally indicates chronic change. From the present result, it was not clear whether the macrophages died because of frustrated phagocytosis.

In an inhalation (nose-only) toxicity test using pigment-sized Fe_3O_4 for Wistar rats, subchronic responses have been reported. Pulmonary inflammation was evidenced by bronchoalveolar lavage (BAL) fluid analysis, histopathology, particle deposition and increased lung and lung-associated lymph node weights at the inhalation doses of 16.6 and 52.1 mg/m^3 [20]. Another report described data from an inhalation study in which male and female Han Wistar rats were exposed to a photocopying toner with an average particle size of 5.1 μm that contained 45–50% magnetite by inhalation for 6 hours/day, 5 days/week, for a total of 13 or 104 weeks[14]. The microscopic findings indicated a mild inflammatory response and infiltration of black-pigmented macrophages in the lungs and the tracheobronchial and mediastinal lymph nodes after 104 weeks of exposure at an inhalation dose of 16 mg/m^3. It is thus suggested that a longer time is required to develop apparent adverse effects, while the responses are generally less severe in the case of administration by inhalation than in the case of administration by instillation. Osier *et al.* compared the response of rats exposed by intratracheal inhalation to titanium dioxide particles with that of rats exposed to similar doses by intratracheal instillation[21]. Animals receiving particles through inhalation showed a decreased pulmonary response, measured by bronchoalveolar lavage parameters, in both severity and persistence when compared with those receiving particles through instillation. These results demonstrate a difference in pulmonary response to an inhaled *vs* an instilled dose, which may be due to differences in dose rate, particle distribution or altered clearance between the two methods. Several experiments have been performed in rats using quartz as a typical lung toxic particle in order to establish an appropriate bioassay for detection of lung damage after particle instillation[22]. The results of those experiments indicated that an intratracheal instillation bioassay system for detection of lung toxicity appeared to be suitable for rapid hazard identification. Even though inhalation is more similar to the exposure route of magnetite in humans than intratracheal instillation, studies using the latter route are still important.

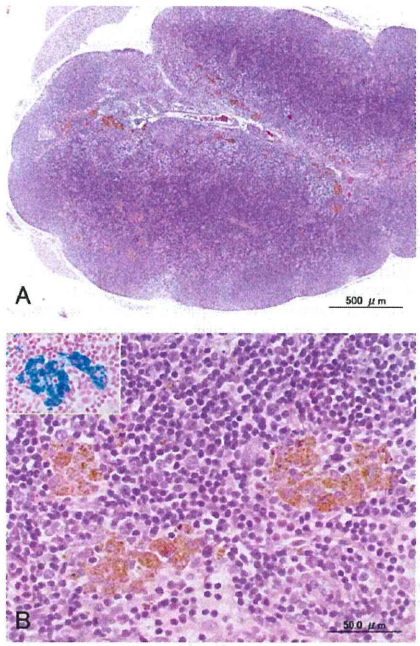

Fig. 5. Representative histologies of the parathymic lymph node (hematoxylin and eosin; inset, Berlin blue) from Fischer 344 rat treated with a single intratracheal spray instillation dose of 15.0 mg/kg body weight of magnetite on day 14. Infiltration of macrophages phagocytosing magnetite and deposits of magnetite particles are evident in rats given the middle dose.

Generally, the acute pulmonary response to foreign bodies is characterized by the inflammation to remove such substances and the resultant cellular debris. If this process is successfully accomplished, complete resolution can occur. On the other hand, if the injury caused by foreign bodies and the subsequent inflammation are severe and sustained due to the persistence of the substances, irreversible pulmonary damage may occur[23]. It is well known that, if the lung is not overloaded with dust, dust-laden macrophages on the alveolar surface migrate upward and are carried by the mucociliary "escalator" system up to the trachea to be cleared into the esophagus. However, when dust enters into the interstitial or subepithelial space of the lung, it becomes very difficult to clear from the lung[24]. Ultrafine particles that penetrate into the lung interstitium make contact with interstitial macrophages and other sensitive cell populations, which is likely to have powerful inflammatory effects that underlie the development of subsequent disease[25]. In the present study, magnetite-laden macrophages were seen not only in the alveolar space but also in the alveolar septa or interstitial space, even in the low-dose group, which indicates the possibility of severe injury resulting from intratracheal administration of magnetite.

In conclusion, these results show that intratracheally administered magnetite nanoparticles cause foreign body inflammatory and granulating lesions in the lung. Magnetite particles are accumulated mainly in the lung and partly translocated to the regional lymph nodes. These pulmonary responses occur in a dose-dependent manner in association with the increase in lung weight.

Acknowledgments: We would like to express our gratitude to Dr. Yukari Totsuka (Cancer Prevention Basic Research Project, National Cancer Center Research Institute, Tokyo, Japan) for arrangement of the supply of magnetite and helpful suggestions. We also thank Mr. Toshiyuki Hakata and the staff of Toda Kogyo Corp. (Otake, Hiroshima, Japan) for their generous supply of magnetite and its technical information. This work was supported in part by a Health and Labour Sciences Research Grant (awarded to Dai Nakae) from the Ministry of Health, Labour and Welfare (MHLW) of Japan.

References

1. Hood E. Nanotechnology: looking as we leap. Environ Health Perspect. **112**: A740–A749. 2004. [Medline] [CrossRef]
2. Torres-Martínez CL, Kho R, Mian OI, and Mehra RK. Efficient photocatalytic degradation of environmental pollutants with mass-produced ZnS nanocrystals. J Colloid Interface Sci. **240**: 525–532. 2001. [Medline] [CrossRef]
3. Lin BL, Shen XD, and Cui S. Application of nanosized Fe_3O_4 in anticancer drug carriers with target-orientation and sustained-release properties. Biomed Mater. **2**: 132–134. 2007. [Medline] [CrossRef]
4. Gang J, Park SB, Hyung W, Choi EH, Wen J, Kim HS, Shul YG, Haam S, and Song SY. Magnetic poly epsilon-caprolactone nanoparticles containing Fe_3O_4 and gemcitabine enhance anti-tumor effect in pancreatic cancer xenograft mouse model. J Drug Target. **15**: 445–453. 2007. [Medline] [CrossRef]
5. Kikumori T, Kobayashi T, Sawaki M, and Imai T. Anti-cancer effect of hyperthermia on breast cancer by magnetite nanoparticle-loaded anti-HER2 immunoliposomes. Breast Cancer Res Treat. **113**: 435–441. 2009. [Medline] [CrossRef]
6. Takada T, Yamashita T, Sato M, Sato A, Ono I, Tamura Y, Sato N, Miyamoto A, Ito A, Honda H, Wakamatsu K, Ito S, and Jimbow K. Growth inhibition of re-challenge B16 melanoma transplant by conjugates of melanogenesis substrate and magnetite nanoparticles as the basis for developing melanoma-targeted chemo-thermo-immunotherapy. J Biomed Biotechnol. **2009**: 457936. 2009. [Medline] [CrossRef]
7. Kawai N, Futakuchi M, Yoshida T, Ito A, Sato S, Naiki T, Honda H, Shirai T, and Kohri K. Effect of heat therapy using magnetic nanoparticles conjugated with cationic liposomes on prostate tumor in bone. Prostate. **68**: 784–792. 2008. [Medline] [CrossRef]
8. Ito A, Tanaka K, Honda H, Abe S, Yamaguchi H, and Kobayashi T. Complete regression of mouse mammary carcinoma with a size greater than 15 mm by frequent repeated hyperthermia using magnetite nanoparticles. J Biosci Bioeng. **96**: 364–369. 2003. [Medline]
9. Xia Z, Wang G, Tao K, Li J, and Tian Y. Preparation and acute toxicology of nano-magnetic ferrofluid. J Huazhong Univ Sci Technolog Med Sci. **25**: 59–61. 2005. [Medline] [CrossRef]
10. Jeng HA, and Swanson J. Toxicity of metal oxide nanoparticles in mammalian cells. J Environ Sci Health A Tox Hazard Subst Environ Eng. **41**: 2699–2711. 2006. [Medline] [CrossRef]
11. Chen BA, Jin N, Wang J, Ding J, Gao C, Cheng J, Xia G, Gao F, Zhou Y, Chen Y, Zhou G, Li X, Zhang Y, Tang M, and Wang X. The effect of magnetic nanoparticles of Fe(3) O(4) on immune function in normal ICR mice. Int J Nanomedicine. **5**: 593–599. 2010. [Medline] [CrossRef]
12. Pott F, Ziem U, Reiffer FJ, Huth F, Ernst H, and Mohr U. Carcinogenicity studies on fibres, metal compounds, and some other dusts in rats. Exp Pathol. **32**: 129–152. 1987. [Medline] [CrossRef]
13. Steinhoff D, Mohr U, and Hahnemann S. Carcinogenesis studies with iron oxides. Exp Pathol. **43**: 189–194. 1991. [Medline] [CrossRef]
14. Slesinski RS, and Turnbull D. Chronic inhalation exposure of rats for up to 104 weeks to a non-carbon-based magnetite photocopying toner. Int J Toxicol. **27**: 427–439. 2008. [Medline] [CrossRef]
15. Zhu MT, Feng WY, Wang B, Wang TC, Gu YQ, Wang M, Wang Y, Ouyang H, Zhao YL, and Chai ZF. Comparative study of pulmonary responses to nano- and submicron-sized ferric oxide in rats. Toxicology. **247**: 102–111. 2008. [Medline] [CrossRef]
16. Zhou YM, Zhong CY, Kennedy IM, and Pinkerton KE. Pulmonary responses of acute exposure to ultrafine iron particles in healthy adult rats. Environ Toxicol. **18**: 227–235. 2003. [Medline] [CrossRef]
17. Japanese Association for Laboratory Animal Science (JALAS) Guidelines for animal experimentation. Exp Anim. **36**: 285–288. 1987.
18. Driscoll KE, Costa DL, Hatch G, Henderson R, Oberdorster G, Salem H, and Schlesinger RB. Intratracheal instillation as an exposure technique for the evaluation of respiratory tract toxicity: uses and limitations. Toxicol Sci. **55**: 24–35. 2000. [Medline] [CrossRef]
19. Gad SC, and Weil CS. Statistics for toxicologist. In: Principles and Methods of Toxicology, 3rd ed. AW Hayes (ed). Raven Press, New York. 221-274. 1994.
20. Pauluhn J. Subchronic inhalation toxicity of iron oxide (magnetite, Fe(3) O(4)) in rats: pulmonary toxicity is determined by the particle kinetics typical of poorly soluble particles. J Appl Toxicol. **32**: 488–504. 2012. [Medline] [CrossRef]
21. Osier M, and Oberdorster G. Intratracheal inhalation vs intratracheal instillation: differences in particle effects. Fundam Appl Toxicol. **40**: 220–227. 1997. [Medline] [CrossRef]
22. Yokohira M, Kuno T, Yamakawa K, Hashimoto N, Ninomiya F, Suzuki S, Saoo K, and Imaida K. An intratracheal instillation bioassay system for detection of lung toxicity due to fine particles in F344 rats. J Toxicol Pathol. **22**: 1–10. 2009. [Medline]
23. Haschek WM, and Witschi HR. Respiratory system. In: Handbook of Toxicologic Pathology, Haschek WM, and Rousseaux CG (eds). Academic Press, San Diego. 761-827. 1991.
24. Lam CW, James JT, McCluskey R, and Hunter RL. Pulmonary toxicity of single-wall carbon nanotubes in mice 7 and 90 days after intratracheal instillation. Toxicol Sci. **77**: 126–134. 2004. [Medline] [CrossRef]
25. Donaldson K, Li XY, and MacNee W. Ultrafine (nanometre particle mediated lung injury. J Aerosol Sci. **29**: 553–560. 1998. [CrossRef]

J Toxicol Pathol 2013; 26: 393–403

Original Article

Long-term Pulmonary Responses to Quadweekly Intermittent Intratracheal Spray Instillations of Magnetite (Fe_3O_4) Nanoparticles for 52 Weeks in Fischer 344 Rats

Yukie Tada[1*], Norio Yano[1], Hiroshi Takahashi[1], Katsuhiro Yuzawa[1], Hiroshi Ando[1], Yoshikazu Kubo[1], Akemichi Nagasawa[1], Akiko Inomata[1], Akio Ogata[1], and Dai Nakae[1,2*]

[1] Department of Pharmaceutical and Environmental Sciences, Tokyo Metropolitan Institute of Public Health, 3-24-1 Hyakunin-cho, Shinjuku, Tokyo 169-0073, Japan
[2] Tokyo University of Agriculture, 1-1-1 Sakura-ga-Oka, Setagaya, Tokyo 156-8502, Japan

Abstract: Information about potential risks of iron nanomaterials is still limited, while a wide variety of applications are expected. We recently reported acute phase responses of male and female Fischer 344 rats after a single intratracheal spray instillation of Fe_3O_4 nanoparticles (magnetite), clearly showing dose-dependent pulmonary inflammatory changes (Tada *et al.*, J Toxicol Pathol 25, 233–239, 2012). The present study assessed long-term responses of male and female Fischer 344 rats to multiple administrations of magnetite. Ten-week-old male and female Fischer 344 rats (n=20/group) were exposed to a total of 13 quadweekly intermittent intratracheal spray instillations of magnetite during the experimental period of 52 weeks, at doses of 0, 0.2 (low), 1.0 (medium) and 5.0 (high-dose) mg/kg body weight per administration. Absolute and relative lung weights of the high-dose group were significantly higher than those of the control group. Macroscopically, slight enlargement and scattered black patches were recognized in the lungs and the lung-associated lymph nodes of the high-dose group. Histopathologically, infiltration of macrophages phagocytosing magnetite (all dose groups) and of chronic inflammatory cells (medium- and high-dose males and high-dose females), alveolar bronchiolization and granuloma (high-dose group) were observed. In addition, alveolar hyperplasias were observed in some rats of the high-dose group, and cytoplasmic overexpression of β-catenin protein was immunohistochemically found in such lesions. The present results clearly show that instilled magnetite causes chronic inflammatory responses in the lung. These responses occur in a dose-dependent manner without apparent differences among sexes (DOI: 10.1293/tox.2013-0036; J Toxicol Pathol 2013; 26: 393–403)

Key words: magnetite, Fe_3O_4, nanoparticles, lung, intratracheal spray instillation, Fischer 344 rat

Introduction

Engineered nanoparticles can have unique photonic and catalytic properties that display great differences from those of over-nanoscaled materials with the same composition. The superb biological and environmental reactivities of nanoparticles have led to their wide and considerable use in disease treatment, pollutant degradation and so forth[1]. Iron nanomaterials are a typical example and are attracting attentions due to their superparamagnetic characteristics and high catalytic abilities. It is expected that iron nanomaterials can be applied to a wide variety of fields such as environmental catalysis, magnetic storage, biomedical imaging[1], magnetic target drug delivery[2] and hyperthermia[3,4].

While information about potential risks of magnetite is still limited, there are several reports describing some toxicologic findings for magnetite[5–13]. In *in vitro* studies using L-929 murine fibroblastic cells, iron oxide nanoparticles affected cell viability and DNA stability[5], while in human alveolar epithelial-like type-II cells (A549), a micronucleus test and comet assay showed genotoxicity of magnetite[6]. *In vivo* studies with Fe_3O_4 particles caused inflammatory changes in rats exposed to pigment-sized particles through inhalation[7,8]. Magnetic nanoparticles of Fe_3O_4 affected the immune system of ICR mice, enhancing production of cytokines like interleukin (IL)-2, interferon-γ and IL-10 (but not IL-4) in the peripheral blood[9]. A high amount of magnetite, 15 mg × 15 intratracheal instillations, unexpectedly resulted in development of lung tumors in female Wistar rats[10], while chronic exposure to iron oxide did not increase the incidence of pulmonary tumors of rats[7,11]. Recently, we reported acute phase responses of male and female Fischer 344 rats 14 days after a single intratracheal spray instillation of magnetite (Fe_3O_4) nanoparticles, clearly showing that magnetite

Received: 3 July 2013, Accepted: 13 August 2013
*Corresponding authors: Y Tada (e-mail: Yukie_Tada@member.metro.tokyo.jp), D Nakae (e-mail: agalennde.dai@nifty.com)

caused foreign body inflammatory and granulating lesions in the lung in a dose-dependent manner[12]. Our histopathological findings showed that magnetite-laden macrophages were seen not only in the alveolar space but also in the alveolar septa or interstitial space, even in the low-dose group given 5.0 mg/kg body weight, indicating the possibility of severe injury resulting from intratracheal administration of magnetite[12].

Iron is a transition metal that is considered to play a pivotal role in modulating oxidative stress and other biological responses[13,14], which are speculated to be the critical mechanisms in eliciting the adverse effects of iron particulate matter exposure. The Organization for Economic Cooperation and Development (OECD) has generated a list of 14 commercially important nanoparticulate materials, in order to explore the possible health effects and regulate occupational and nonoccupational exposure scenarios, and iron oxide is included in the list[15]. In this context, it is apparently important to accumulate data regarding the toxicity/safety of magnetite, especially for its chronic influence on the living organisms. The present study was thus conducted to assess pulmonary responses to long-term intermittent intratracheal spray instillations of Fe_3O_4 nanoparticles (magnetite) in male and female Fischer 344 rats.

Materials and Methods

Ethical considerations

The current study was performed principally in conformity with the Guidelines for the Toxicity Testing of Pharmaceuticals released by the Ministry of Health, Labour and Welfare of Japan (http://www.pmda.go.jp/ich/s/s4_93_8_10.pdf; http://www.pmda.go.jp/ich/s/s4a_99_4_5.pdf). The experimental protocol was approved by the Experiments Regulation Committee and Animal Experiment Committee of the Tokyo Metropolitan Institute of Public Health, prior to its execution. All the animals were handled in accordance with the Japanese Government Animal Protection and Management Law, Japanese Government Notification on Feeding and Safekeeping of Animals and the Guidelines for Animal Experimentation issued by the Japanese Association for Laboratory Animal Science[16].

Animals

A total of 168 male and female specific pathogen-free Fischer 344 (F344/DuCrlCrlj) rats were purchased at 8 weeks of age from Charles River Laboratories Japan, Inc. (Kanagawa, Japan). The rats were housed individually in stainless steel cages and were kept under controlled conditions of temperature (22–24°C), relative humidity (50–60%) and ventilation (more than 10 times/hour) with a 12-hr light/dark cycle. They were allowed free access to pelleted chow CE-2 (CLEA Japan, Inc., Tokyo, Japan) and drinking water throughout both the acclimation and experimental periods. After confirming normal health status at the end of the 2-week acclimation period, 80 rats of each sex were selected for use and randomly allocated to 4 groups of 20 rats. The rats were observed twice daily, and clinical signs and mortality were recorded. Body weight and food intakes were monitored weekly during the first 13 weeks, and were monitored every four weeks thereafter.

Test chemical and animal treatments

The magnetite slurry (Fe_3O_4 nanoparticle suspension; lot numbers, 90828 and 100316) was generously supplied by Toda Kogyo Corp. (Hiroshima, Japan). A representative transmission electron microscopic view of magnetite particles is shown in Fig. 1, and the primary particle size of the prepared sample was estimated to be 5–15 nm in diameter. The specific surface areas were determined to be 116.0 and 122.0 m^2/g for lot numbers 90828 and 100316, respectively, by the BET method. The purity of the test chemical was determined by an energy dispersive X-ray spectrometer, and only iron and oxygen were detected. Magnetite particles are poorly soluble in water. According to our previous report[12], magnetite slurry was diluted in sterile ultrapure water (vehicle: Milli-Q water, 18.2 MΩ) and adjusted to pH 7.4 with 0.1 M hydrochloric acid.

The intratracheal instillation technique was performed according to the recommendations of Driscoll *et al.*[17]. Before intratracheal spray instillation, the rats were anesthetized with diethyl ether and placed in a supine position on an angled board with their necks extended. Magnetite suspension was placed in an ultrasonication bath (Sonorex RK31, Bandelin Electronic, Berlin, Germany) set at a high frequency (35 kHz) and then inserted via the mouth into the bifurcation of trachea by a sterile stainless steel tube (IA-1B MicroSprayer, Penn-Century, Inc., Wyndmoor, PA, USA) at the concentrations of 0 (control: vehicle, 1.0 mL/kg body weight), 0.2 (low), 1.0 (medium) and 5.0 (high) mg/kg body weight, and this was followed by insufflation of 0.2 mL of air. The doses were decided based on the finding of

Fig. 1. Representative transmission electron microscopic view of magnetite nanoparticles. The estimated primary particle size is about 5–15 nm in diameter.

our acute single-dose toxicity study[12] showing that 15 mg/kg body weight of magnetite cannot be well dispersed in the lung and thus aggregated and filled in the alveoli. The rats were given a total of 13 quadweekly intermittent exposures during the experimental period of 52 weeks.

Animal sacrifice and assessments

Four weeks after the last instillation, all rats were deprived of food (but not water) overnight, and fresh urine samples were obtained for urinalysis of urobilinogen, occult blood, bilirubin, ketone, glucose, protein and pH using test papers (N-Multistix, Siemens Healthcare Diagnostics Inc., Tokyo, Japan). The rats were then lightly anesthetized by diethyl ether and sacrificed by exsanguination after collecting blood samples via the abdominal aorta. The blood for hematology was collected into tubes treated with dipotassium ethylenediaminetetraacetate. The hematological examination was carried out using an automatic analyzer (Sysmex KX-21NV, Sysmex Corporation, Hyogo, Japan) to determine the red blood cell count (RBC), hemoglobin concentration (HGB), hematocrit level (HCT), mean corpuscular volume (MCV), mean corpuscular hemoglobin (MCH), mean corpuscular hemoglobin concentration (MCHC), white blood cell count (WBC) and platelet count (PLT). A serum biochemistry analysis was performed with an automatic analyzer (TBA-120FR, Toshiba Medical Systems Corporation, Tokyo, Japan) to determine the levels of total protein (TP), albumin (ALB), albumin/globulin ratio (A/G), glucose (GLU), total cholesterol (T-CHO), triglyceride (TG), total bilirubin (T-BIL), aspartate aminotransferase (AST), alanine aminotransferase (ALT), alkaline phosphatase (ALP), blood urea nitrogen (BUN), creatinine (CRE), uric acid (UA), sodium (Na), potassium (K), chlorine (Cl) and calcium (Ca).

Upon sacrifice, the rats were macroscopically examined and subjected to a full autopsy. The brain, thyroids (with parathyroids), adrenal glands, lungs (including bronchi, fixed by inflation with fixative), heart, spleen, liver, kidneys, testes, ovaries and uterus were weighed and fixed in 10% neutrally buffered formalin. As well as these organs, the pituitary gland, sciatic nerve, spinal cords (cervical, mid-thoracic and lumbar), eyes, harderian glands, Zymbal's glands, thoracic aorta, nasal cavity, trachea, thymus, salivary glands, tongue, esophagus, stomach, duodenum, jejunum, ileum, caecum, rectum, pancreas, urinary bladder, epididymides, seminal vesicles, prostate, preputial glands, oviducts, vagina, skin with mammary glands, skeletal muscle, lymph nodes (submandibular and mesenteric), bones (femur and sternum) with bone marrow and all gross lesions of each animal were fixed. Paraffin-embedded sections were routinely prepared and histopathologically examined after being stained with hematoxylin and eosin, Azan-Mallory and Berlin blue procedures.

Immunohistochemistry was performed on 4-μm sections of the formalin-fixed paraffin embedded tissues, using a monoclonal mouse antibody to β-catenin (610153, BD Biosciences, San Jose, CA, USA). Heat-induced antigen retrieval with 10 mM citrate buffer, pH 6.0, was followed by incubation with the primary antibody (diluted to 1:100) at room temperature for 30 minutes. Detection of primary antibody binding was carried out with an EnVision antimouse/horseradish peroxidase-labeled polymer detection system (Dako North America Inc., Carpinteria, CA, USA) followed by visualization with 3,3'-diaminobenzidine (DAB) (Dako) and counterstaining with Mayer's hematoxylin. Negative control slides were subjected to the same staining protocol modified by the substitution of mouse normal IgG for the primary antibody.

Statistical analysis

For numerical data such as body and organ weights and hematological and serological outcomes, equality was assessed by Bartlett's test. Homogeneity of variance was then analyzed by one-way analysis of variance, and finally differences between the values of the control group and those of each treated group were evaluated by Dunnett's test. If the Bartlett's test was significant, the data were subjected to the Kruskal-Wallis test and Dunnett's-type rank sum test. For contingent data such as incidences of histopathological lesions, differences between the values of the control group and those of each treated group were evaluated by Fisher's exact probability test[18]. Statistical processing was conducted using the StatLight software (Yukms Co., Ltd., Tokyo, Japan). Intergroup differences were considered statistically significant, when P values less than 0.05 were obtained.

Results

General findings

Rats given magnetite (especially at the high dose) became less active than controls after instillation but recovered relatively soon. During the study, however, 3 low-dose males, 3 control females and 1, 2 and 4 low-, medium- and high-dose females, respectively, died due to deep anesthesia following magnetite administration. In addition, accidental deaths due to suffocation with the diet occurred in 3 medium-dose males, 3 control females and 2, 1 and 4 low-, medium- and high-dose females, respectively. As a result, the final effective numbers of rats were 20, 17, 17 and 20 for males and 14, 17, 17 and 12 for females in the control group and low-, medium- and high-dose groups, respectively. There were no significant differences in average body weights among groups throughout the experimental period for either sex (Fig. 2).

Urinalysis, hematology and serum biochemistry

In the urinalysis, no significant or treatment-related changes were observed in any analyzed parameters.

In the hematology, the MCHC values of the female control and low-, medium- and high-dose groups were 34.1 ± 0.8, 34.3 ± 0.6, 34.0 ± 0.6 and 33.4 ± 0.3 g/dL, respectively. Although the female high-dose value was significantly lower than the female control value, the change must lack a biological meaning or relation to the magnetite exposure,

because the slight decrease was not accompanied by any other hematological, serological or pathological relatedness. The WBC values of the male control and low-, medium- and high-dose groups were 32.8 ± 7.3, 30.0 ± 7.0, 30.0 ± 6.7 and 37.1 ± 10.7 $\times 10^2/\mu L$, respectively. The WBC values of the female control and low-, medium- and high-dose groups were 21.7 ± 6.1, 23.1 ± 6.6, 18.1 ± 3.5 and 21.8 ± 5.4 $\times$ $10^2/\mu L$, respectively. There were no significant differences in WBC data between the control and treated groups. No significant or treatment-related changes were observed in any other analyzed parameters.

In the serum biochemistry, the GLU values of the male control and low-, medium- and high-dose groups were 155.1 ± 16.6, 142.8 ± 15.5, 144.9 ± 15.5 and 139.1 ± 13.2 mg/dL, respectively, and the male low- and high-dose values were significantly lower than the male control value. The Na values of the male control and low-, medium- and high-dose groups were 140.8 ± 1.1, 141.3 ± 1.9, 141.7 ± 1.7 and 143.0 ± 1.6 mmol/L, respectively, and the male high-dose value was significantly higher than the male control value. The Na values of the female control and low-, medium- and high-dose groups were 141.4 ± 1.8, 142.6 ± 2.0, 144.7 ± 1.7 and 143.8 ± 1.3 mmol/L, respectively, and the female medium- and high-dose values were significantly higher than the female control group value. The Cl values of the male control and low-, medium- and high-dose groups were 104.6 ± 1.3, 105.8 ± 0.6, 105.4 ± 0.8 and 106.8 ± 1.0 mmol/L, respectively, and the male low- and high-dose values were significantly higher than the male control value. The Cl values of the female control and low-, medium- and high-dose groups were 105.8 ± 1.7, 106.2 ± 2.1, 108.2 ± 2.8 and 107.7 ± 1.6 mmol/L, respectively, and the female medium-dose value was significantly higher than the female control value. The Ca values of the female control and low-, medium- and high-dose groups were 10.2 ± 0.3, 10.5 ± 0.3, 10.4 ± 0.3 and 10.4 ± 0.3 mg/dL, respectively, and the female low- and medium- dose values were significantly higher than the female control value. These slight changes must lack a biological meaning or relation to the magnetite exposure, because they were not accompanied any other hematological, serological or pathological relatedness, and frequently did not show first-order dose-dependency. No significant or treatment-related changes were observed in any other analyzed parameters.

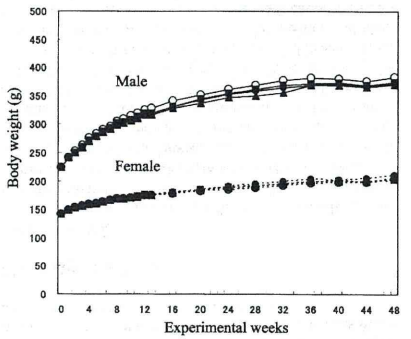

Fig. 2. Changes in mean body weights determined quadweekly for 52 weeks. The doses of magnetite were 0 (control) ○, 0.2 ●, 1.0 ▲ or 5.0 ■ mg/kg body weight per administration.

Pathology

While initial or final body weights were not different among groups, both absolute and relative lung weights of the high-dose group were significantly higher than the control value in both sexes (Table 1). The absolute weights of the thyroid glands of the male control and low-, medium- and high-dose groups were 21.0 ± 3.5, 17.7 ± 2.5, 21.4 ± 5.3 and 18.6 ± 2.2 mg, while their relative weights were 5.7 ± 0.8, 5.0 ± 0.7, 6.1 ± 1.7 and 5.2 ± 0.6 mg/100 g body weight, respectively, and the male low-dose values were significantly lower than the respective male control values. On the other hand, the absolute weights of the thyroid glands of the female control and low-, medium- and high-dose groups were 13.2 ± 3.0, 12.6 ± 3.0, 15.7 ± 3.1 and 13.1 ± 1.9 mg, while their relative weights were 6.9 ± 1.2, 6.4 ± 1.4, 8.2 ± 1.6 and 6.7 ± 0.8 mg/100 g body weight, respectively, and the female medium-dose values were significantly higher than the respective female control values. These slight changes in the thyroid gland weights must lack a biological meaning or relation to the magnetite exposure, because they were not accompanied any other hematological, serological or pathological relatedness, and did not show first-order dose-dependency. No significant or treatment-related changes were observed in any other organ weights.

Table 1. Initial and Final Body Weights and Lung Weights

Item	Dose of magnetite (mg/kg body weight)			
	0 (control)	0.2	1.0	5.0
Male				
Initial number of rats	20	20	20	20
Initial body weight (g)	224.1 ± 8.2[a]	223.5 ± 8.8	224.1 ± 7.9	223.4 ± 7.0
Final effective number of rats	20	17	17	20
Final body weight (g)	383.3 ± 20.3	372.1 ±20.1	370.0 ± 29.4	374.9 ± 23.0
Absolute lung weight (mg)	1017.4 ± 95.0	963.6 ± 57.8	1015.3 ± 60.7	1380.0 ± 82.2*
Relative lung weight (mg/100 g body weight)	278.7 ± 25.3	274.0 ± 17.5	289.8 ± 27.4	387.4 ± 24.1*
Female				
Number of rats	20	20	20	20
Initial body weight (g)	141.8 ± 4.9	141.4 ± 6.5	142.0 ± 5.5	142.2 ± 5.6
Final effective number of rats	14	17	17	12
Final body weight (g)	203.2 ± 17.8	210.9 ± 19.4	205.2 ± 19.2	202.6 ± 22.1
Absolute lung weight (mg)	729.3 ± 50.7	732.3 ± 63.5	722.3 ± 50.7	1086.2 ± 102.8*
Relative lung weight (mg/100 g body weight)	385.1 ± 45.1	372.5 ± 36.7	378.3 ± 40.5	559.0 ± 51.9*

[a] Values are means ± standard deviations, except those for animal numbers. * Significantly different from the corresponding control values (P<0.05, Dunnett's test).

An apparent macroscopic finding was obtained at necropsy in the high-dose groups of both sexes, with the lungs being slightly enlarged in association with dark brown patches scattered in almost all their lobes (Fig. 3). Additionally, dark brown patches were also observed in the parathymic lymph nodes of male and female rats in the high-dose groups. No significant or treatment-related changes were macroscopically observed in any other organs or tissues.

The histopathological changes detected in the lungs are summarized in Table 2. In the lungs of all rats in all magnetite-treated groups, infiltration of brownishly pigmented macrophages phagocytosing magnetite was observed in the alveolar spaces, walls and interstitium (Figs. 4B, 4C, 4D). Such infiltration was not present in the control groups, and among the magnetite-treated groups, the severity of this change generally increased with the increasing doses of magnetite. Chronic inflammation was observed in 4/17 (23.5%) and 20/20 (100%) of the medium- and high-dose males and 3/17 (17.6%; statistically insignificant), 3/17 (17.6%; statistically insignificant) and 12/12 (100%) of the low-, medium- and high-dose females, respectively. The chronic inflammation was evidenced by an infiltration of inflammatory cells, such as lymphocytes or neutrophils, and fibrosis. This chronic inflammation was frequently associated with macrophages (either phagocytosing magnetite or not) diffusely scattered within the alveolar lumens, and thence multiple focal clusters of alveoli filled with inflammatory cells (mostly macrophages but occasionally mixed with small to moderate numbers of neutrophils) were commonly observed with debris (Figs. 5A, 5B). Hypertrophy and hyperplasia of alveolar epithelial cells (presumably type II pneumocytes) were usually seen in alveoli containing such inflammatory exudates, which were not considered separate/independent lesions but regenerative responses secondary to the inflammation. Alveolar bronchiolization, identified by the lining of normal or thickened alveolar walls with cells resembling the bronchiolar epithelium (Figs. 5C, 5D), was observed in 2/17 (11.8%; statistically insignificant) and 15/20 (75.0%) of the medium- and high-dose males and 3/17 (17.6%; statistically insignificant) and 12/12 (100%) of the medium- and high-dose females, respectively. The bronchiolized epithelium consisted of a single layer of ciliated and nonciliated columnar cells, and extended from the terminal bronchiole onto the septa of the adjacent alveoli (Figs. 5C, 5D). As an additional inflammatory change, granuloma was observed in 7/20 (35%) and 6/12 (50%) of the high-dose males and females, respectively. On the other hand, alveolar

Table 2. Histological Findings of the Lungs and Parathymic Lymph Nodes

Item	Dose of magnetite (mg/kg body weight)			
	0 (control)	0.2	1.0	5.0
Male				
Effective number of rats	20	17	17	20
Lung				
Infiltration of macrophages phagocytosing magnetite	0[a]	17*	17*	20*
Chronic inflammation	0	0	4*	20*
Alveolar bronchiolization	0	0	2	15*
Granuloma	0	0	0	7*
Bronchoalveolar hyperplasia	3	0	0	2
Parathymic lymph nodes				
Infiltration of macrophages phagocytosing magnetite	0	17*	17*	20*
Female				
Effective number of rats	14	17	17	12
Lung				
Infiltration of macrophages phagocytosing magnetite	0	17*	17*	12*
Chronic inflammation	0	3	3	12*
Alveolar bronchiolization	1	0	3	12*
Granuloma	0	0	0	6*
Bronchoalveolar hyperplasia	0	0	0	2
Parathymic lymph nodes				
Infiltration of macrophages phagocytosing magnetite	0	17*	17*	12*

[a] Number of rats with a lesion. * Significantly different from the corresponding control values (P<0.05, Fisher's exact test). No apparent histological changes were observed in the other organs when compared with the control rats.

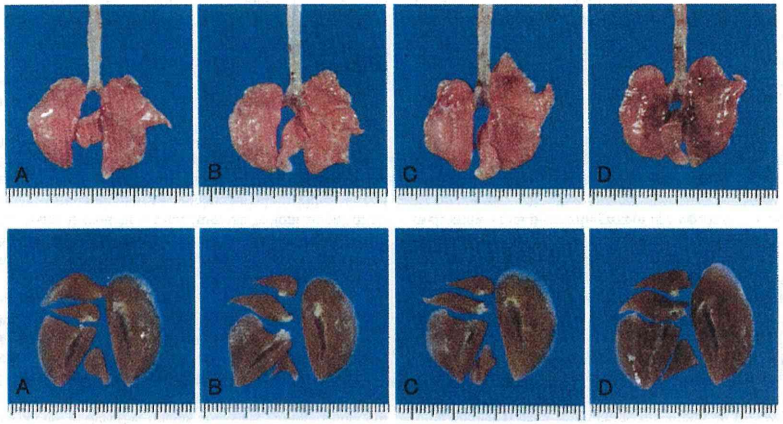

Fig. 3. Representative gross views (upper row) and cross-sections of the formalin-fixed tissues (lower row) of the lungs. The doses of magnetite were 0 (control) (A), 0.2 (B), 1.0 (C) and 5.0 (D) mg/kg body weight per administration.

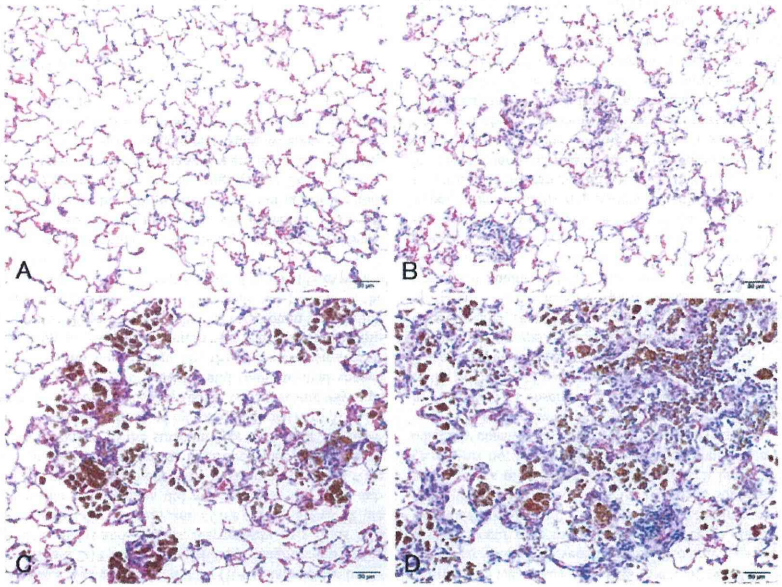

Fig. 4. Representative microscopic views of the lungs of the control (A) and low- (B), medium- (C) and high-dose (D) groups (hematoxylin and eosin).

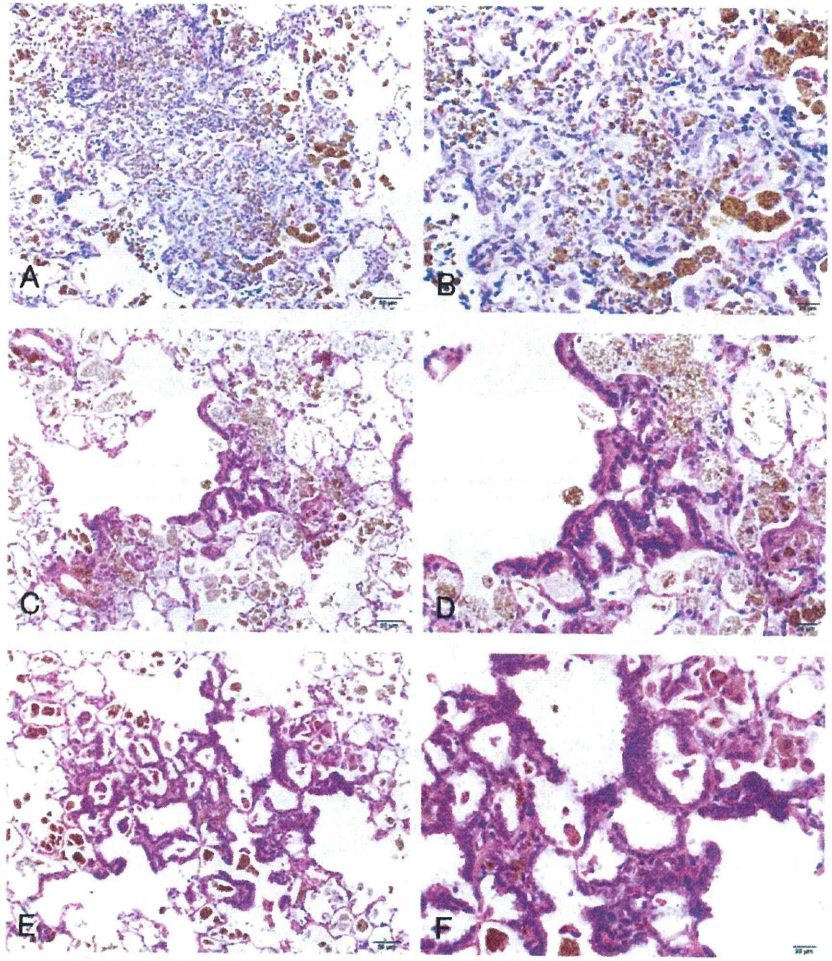

Fig. 5. Representative lesions observed in the lungs of the high-dose group (hematoxylin and eosin): infiltration of macrophage phagocytosing magnetite (A–F), chronic inflammation (A, B), alveolar bronchiolization (C, D) and alveolar hyperplasia (E, F). The right row shows higher magnification versions of the left row images. The bronchiolization was identified as a non-proliferative lesion, in which the lining of alveolar walls was replaced by cells resembling the bronchiolar epithelium. The alveolar hyperplasia was identified as a lesion consisting of proliferative alveolar epithelial cells.

hyperplasia was observed in 2/20 (10%; statistically insignificant) and 2/12 (16.7%; statistically insignificant) of the high-dose males and females, respectively, as well as 3/20 (15%; statistically insignificant) of the control males. While the alveolar hyperplasias did not compress the surrounding parenchyma, those observed in the control males were focal, and those found in the high-dose males and females tended to extend to the surroundings with poor demarcation and were accompanied by inflammation (Figs. 5E, 5F). The hyperplastic alveolar epithelial cells (presumably type II pneumocytes) were cuboidal and round-to-oval shaped hyperchromatic nuclei (Figs. 5E, 5F), and cytoplasmic overexpression of β-catenin protein was immunohistochemically found (Figs. 6C, 6D), whereas the protein was mainly localized at the membranes of the cell-cell borders in the background lung tissue irrespective of magnetite exposure (Figs. 6A, 6B).

In the parathymic lymph nodes, infiltration of macrophages phagocytosing magnetite was observed in all rats in all magnetite-treated groups (Fig. 7) but not in the control animals, as shown in the lungs (Table 2). No significant or treatment-related changes were histopathologically observed in any other organs or tissues, whereas sporadic spontaneous lesions were observed identically in the control and treated rats.

Discussion

The present study clearly revealed that a total of 13 quadweekly intermittent intratracheal spray instillations of magnetite (Fe_3O_4) nanoparticles for 52 weeks at doses of 0, 0.2, 1.0 and 5.0 mg/kg body weight per administration caused dose-dependent inflammatory changes in the lung and parathymic lymph node of male and female Fischer 344 rats but not in the other organs or tissues. A large amount of the administered magnetite remained in the lung, and some of the magnetite was distributed into the regional lymph nodes. Histopathologically, infiltration of macrophages phagocytosing magnetite and of chronic inflammatory cells, alveolar bronchiolization and granuloma were observed in the lungs of treated rats.

Alveolar bronchiolization is identified as cells resembling a bronchiolar epithelia line on normal or thickened alveolar walls, which often manifest an acinar formation[19]. This lesion is thought to arise from the "colonization" of alveolar walls within the bronchiolar epithelium either via cell migration through alveolar pores or from the transformation of alveolar type II cells into bronchiolar-type epithelium[19]. This is seen in various types of experimental lung injury caused by viral infection[20] or exposure to ozone[21], chromate[19] and paraquat[22]; it is also seen in human lung cancer cases[23]. Jensen-Taubman *et al.* examined the incidence and association of alveolar bronchiolization with non-small cell lung cancer (NSCLC) in lung resection specimens from 2 patient groups, those with NSCLC and those diagnosed with a variety of non-neoplastic lung conditions[23]. They observed that alveolar bronchiolization occurs in up to 8% (1/12) of non-lung-cancer cases and 12% (5/42) of NSCLC cases. They described that alveolar bronchiolization does not necessarily occur only in adenocarcinoma cases, suggesting that this form of alveolar metaplasia may somehow be associated with a spectrum of NSCLC histologic subtypes. The precise roles of alveolar bronchiolization in lung carcinogenesis are not known at this moment, and thus this lesion is currently considered to be an inflammatory response.

In line with the content of the last paragraph, alveolar hyperplasia was observed in male and female rats exposed to the high dose of magnetite, whereas the incidences were low and not significantly different from those in the respective control groups. A similar lesion was observed also in control males (but not females), but the histopahological appearances of the lesions seen in the treated groups were somewhat qualitatively different from those seen in male control animals. A "primary" alveolar hyperplasia is considered a precursor lesion of lung cancers and must be differentiated from regenerative hyperplasia. A preneoplastic hyperplasia is usually not associated with inflammation or necrosis, and the parenchymal architecture is maintained[24]. While alveolar hyperplasias seen in the high-dose groups of the present study were accompanied by chronic inflammation, a number of molecular pathways activated in chronic inflammation have been indicated to contribute to lung carcinogenesis[25]. Alveolar epithelial cells contribute to the initiation and modulation of inflammatory responses, which in turn may result in the release of cytokines, growth factors and other peptide mediators that may predispose epithelial cells themselves to a proliferative response[26,27]. Foreign particles, infectious agents and chemicals can induce an inflammatory response in the lung leading to oxidative stress. Also with regard to magnetite, exposure to it has been shown to induce oxidative stress and deplete antioxidant levels in the lung epithelial cells, stimulating the apoptotic pathway for cell death[14]. Furthermore, magnetite particles have been revealed to induce concentration-dependent DNA damage and enhance reactive oxygen species production[6] and micronuclei induction[28]. It may be particularly of importance that β-catenin protein was overexpressed in the epithelial cells of the presently observed alveolar hyperplasia in the high magnetite dose groups, while the protein was localized in the membranes of the cell-cell borders of the background lung tissue irrespective of magnetite exposure. It is very well known that β-catenin protein is a versatile component of homotypic cell adhesion and signaling, the subcellular localization and cytoplasmic levels of which are tightly regulated by adenomatous polyposis coli (APC) protein. Mutations occurring in the *β-catenin* and/or *APC* genes result in aberrant overexpression of β-catenin protein first in the cytoplasms and then its translocation into the nuclei, causing nuclear accumulation of the protein and in turn improper gene activation[29]. Typically, for instance, the accumulated β-catenin protein in the nuclei interacts with the Tcf family members, resulting in the acquisition of growth advantage of target genes[30]. Likewise, immunohistochemical studies of *N*-nitrosobis (2-hydroxypropyl) amine-induced rat lung

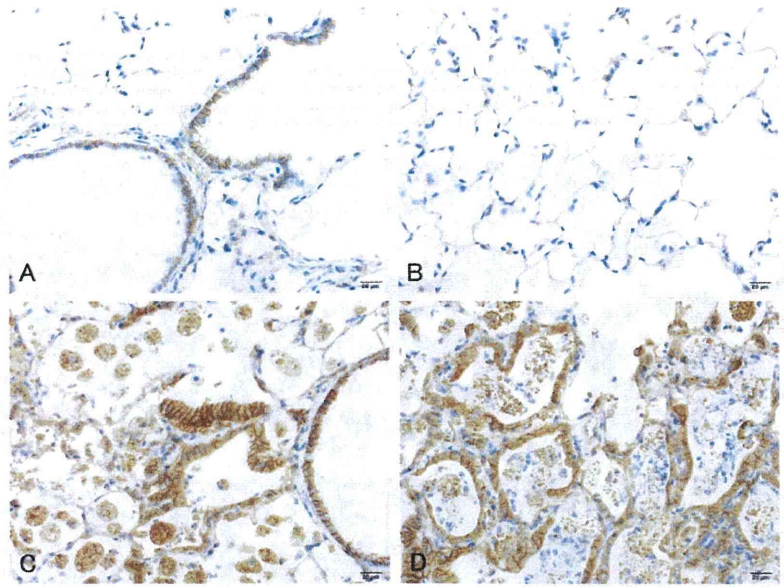

Fig. 6. Representative results of β-catenin immunohistochemistry of the lungs of the control (A, B) and high-dose (C, D) groups. The β-catenin protein was localized at the membranes of the cell-cell borders in the background lung tissue (A–D), whereas cytoplasmic overexpression of the protein was found in the hyperplastic alveolar epithelial cells (C, D).

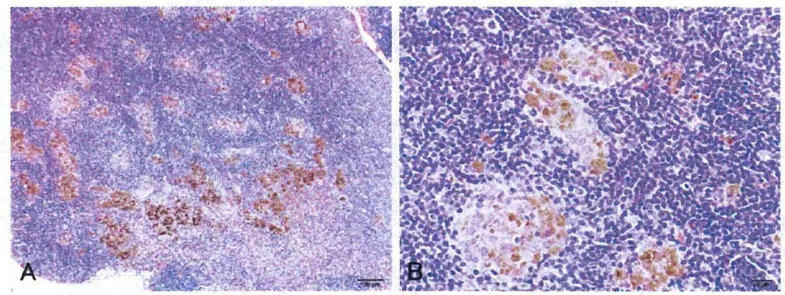

Fig. 7. Representative microscopic views of the parathymic lymph node of the high-dose group (hematoxylin and eosin). Infiltration of macrophages phagocytosing magnetite and deposits of magnetite particles are evident.

tumors[30] and of azoxymethane-induced rat colon tumors[31,32] have revealed frequent translocation of the β-catenin protein from the cell membranes to the cytoplasms and then the nuclei in adenomas and adenocarcinomas, but not in hyperplasia, suggesting the mechanistic involvement of the nuclear accumulation of the protein in those chemical carcinogenesis processes. In this context, the presently observed alveolar hyperplasias in rats exposed to the high dose of magnetite might possess a potent preneoplastic potential. When considering the potential risk for humans, therefore, further studies are apparently warranted to elucidate whether or not intratracheally administered magnetite has the potency to cause lung carcinogenesis, and such studies are being conducted in our laboratories.

In conclusion, the present results clearly show that instilled magnetite causes chronic inflammatory responses in the lung. These long-term pulmonary responses occur in a dose-dependent manner without apparent differences among sexes.

Acknowledgments: The authors would like to express their gratitude to Dr. Yukari Totsuka (Cancer Prevention Basic Research Project, National Cancer Center Research Institute, Tokyo, Japan) for arrangement of the supply of magnetite and helpful suggestions. We also thank Mr. Toshiyuki Hakata and the staff of Toda Kogyo Co., Inc. (Hiroshima, Japan), for their generous supply of magnetite and its technical information. This work was supported in part by a Health and Labour Sciences Research Grant (awarded to Dai Nakae) from the Ministry of Health, Labour and Welfare of Japan.

References

1. Hood E. Nanotechnology: looking as we leap. Environ Health Perspect. **112**: A740–A749. 2004. [Medline] [CrossRef]
2. Lin BL, Shen XD, and Cui S. Application of nanosized Fe_3O_4 in anticancer drug carriers with target-orientation and sustained-release properties. Biomed Mater. **2**: 132–134. 2007. [Medline] [CrossRef]
3. Kikumori T, Kobayashi T, Sawaki M, and Imai T. Anti-cancer effect of hyperthermia on breast cancer by magnetite nanoparticle-loaded anti-HER2 immunoliposomes. Breast Cancer Res Treat. **113**: 435–441. 2009. [Medline] [CrossRef]
4. Hilger I, and Kaiser WA. Iron oxide-based nanostructures for MRI and magnetic hyperthermia. Nanomedicine (Lond). **7**: 1443–1459. 2012. [Medline] [CrossRef]
5. Hong SC, Lee JH, Lee J, Kim HY, Park JY, Cho J, Lee J, and Han DW. Subtle cytotoxicity and genotoxicity differences in superparamagnetic iron oxide nanoparticles coated with various functional groups. Int J Nanomedicine. **6**: 3219–3231. 2011. [Medline]
6. Könczöl M, Ebeling S, Goldenberg E, Treude F, Gminski R, Gieré R, Grobéty B, Rothen-Rutishauser B, Merfort I, and Mersch-Sundermann V. Cytotoxicity and genotoxicity of size-fractionated iron oxide (magnetite) in A549 human lung epithelial cells: Role of ROS, JNK, and NF-κB. Chem Res Toxicol. **24**: 1460–1475. 2011. [Medline] [CrossRef]
7. Slesinski RS, and Turnbull D. Chronic inhalation exposure of rats for up to 104 weeks to a non-carbon-based magnetite photocopying toner. Int J Toxicol. **27**: 427–439. 2008. [Medline] [CrossRef]
8. Pauluhn J. Subchronic inhalation toxicity of iron oxide (magnetite, Fe_3O_4) in rats: pulmonary toxicity is determined by the particle kinetics typical of poorly soluble particles. J Appl Toxicol. **32**: 488–504. 2012. [Medline] [CrossRef]
9. Chen BA, Jin N, Wang J, Ding J, Gao C, Cheng J, Xia G, Gao F, Zhou Y, Chen Y, Zhou G, Li X, Zhang Y, Tang M, and Wang X. The effect of magnetic nanoparticles of Fe_3O_4 on immune function in normal ICR mice. Int J Nanomedicine. **5**: 593–599. 2010. [Medline] [CrossRef]
10. Pott F, Ziem U, Reiffer FJ, Huth F, Ernst H, and Mohr U. Carcinogenicity studies on fibres, metal compounds, and some other dusts in rats. Exp Pathol. **32**: 129–152. 1987. [Medline] [CrossRef]
11. Steinhoff D, Mohr U, and Hahnemann S. Carcinogenesis studies with iron oxides. Exp Pathol. **43**: 189–194. 1991. [Medline] [CrossRef]
12. Tada Y, Yano N, Takahashi H, Yuzawa K, Ando H, Kubo Y, Nagasawa A, Ogata A, and Nakae D. Acute phase pulmonary responses to a single intratracheal spray instillation of magnetite (Fe_3O_4) nanoparticles in Fischer 344 rats. J Toxicol Pathol. **25**: 233–239. 2012. [Medline] [CrossRef]
13. Singh N, Jenkins GJ, Asadi R, and Doak SH. Potential toxicity of superparamagnetic iron oxide nanoparticles (SPION). Nano Rev. **1**: 5358–5373. 2010. [Medline]
14. Ramesh V, Ravichandran P, Copeland CL, Gopikrishnan R, Biradar S, Goornavar V, Ramesh GT, and Hall JC. Magnetite induces oxidative stress and apoptosis in lung epithelial cells. Mol Cell Biochem. **363**: 225–234. 2012. [Medline] [CrossRef]
15. Organisation for Economic Co-operation and Development (OECD). List of Manufactured Nanomaterials and List of Endpoints for Phase One of the Sponsorship Programme for the Testing of Manufactured Nanomaterials: Revision. Paris. 1–16. 2010.
16. Japanese Association for Laboratory Animal Science (JALAS) Guidelines for animal experimentation. Exp Anim. **36**: 285–288. 1987.
17. Driscoll KE, Costa DL, Hatch G, Henderson R, Oberdorster G, Salem H, and Schlesinger RB. Intratracheal instillation as an exposure technique for the evaluation of respiratory tract toxicity: uses and limitations. Toxicol Sci. **55**: 24–35. 2000. [Medline] [CrossRef]
18. Gad SC, and Weil CS. Statistics for toxicologist. In: Principles and Methods of Toxicology, 3rd ed. AW Hayes (ed). Raven Press, New York. 221–274. 1994.
19. Nettesheim P, and Szakal AK. Morphogenesis of alveolar bronchiolization. Lab Invest. **26**: 210–219. 1972. [Medline]
20. Baskerville A, Thomas G, Wood M, and Harris WJ. Histology and ultrastructure of metaplasia of alveolar epithelium following infection of mice and hamsters with influenza virus. Br J Exp Pathol. **55**: 130–137. 1974. [Medline]
21. Pinkerton KE, Dodge DE, Cederdahl-Demmler J, Wong VJ, Peake J, Haselton CJ, Mellick PW, Singh G, and Plopper CG. Differentiated bronchiolar epithelium in alveolar ducts of rats exposed to ozone for 20 months. Am J Pathol. **142**: 947–956. 1993. [Medline]

22. Fukuda Y, Takemura T, and Ferrans VJ. Evolution of metaplastic squamous cells of alveolar walls in pulmonary fibrosis produced by paraquat. Virchows Arch B. **58**: 27–43. 1989. [Medline] [CrossRef]
23. Jensen-Taubman SM, Steinberg SM, and Linnoila RI. Bronchiolization of the alveoli in lung cancer: pathology, patterns of differentiation and oncogene expression. Int J Cancer. **75**: 489–496. 1998. [Medline] [CrossRef]
24. Dixon D, Herbert RA, Sills RC, and Boorman GA. Lungs, pleura, and mediastinum. In: Pathology of the Mouse: Reference and Atlas. RR Maronpot, GA Boorman, and BW Gaul (eds). Cache River, Vienna. 293-332. 1999.
25. Ballaz S, and Mulshine JL. The potential contributions of chronic inflammation to lung carcinogenesis. Clin Lung Cancer. **5**: 46–62. 2003. [Medline] [CrossRef]
26. Simon RH, and Paine R. Participation of pulmonary alveolar epithelial cells in lung inflammation. J Lab Clin Med. **126**: 108–118. 1995. [Medline]
27. Shacter E, and Weitzman SA. Chronic inflammation and cancer. Oncology. **16**: 217–226, 229–232. 2002. [Medline]
28. Kawanishi M, Ogo S, Ikemoto M, Totsuka Y, Ishino K, Wakabayahsi K, and Yagi T. Genotoxicity and reactive oxygen species production induced by magnetite nanoparticles in mammalian cells. J Toxicol Sci. 2013; in press. [Medline] [CrossRef]
29. Ilyas M, and Tomlinson IPM. The interactions of APC, E-cadherin and β-catenin in tumor development and progression. J Pathol. **182**: 128–137. 1997. [Medline] [CrossRef]
30. Tsujiuchi T, Tsutsumi M, Sasaki Y, Murata N, and Konishi Y. Mutations of adenomatous polyposis coli and beta-catenin genes during progression of lung tumors induced by *N*-nitrosobis(2-hydroxypropyl)amine in rats. Cancer Res. **60**: 6611–6616. 2000. [Medline]
31. Takahashi M, Fukuda K, Sugimura T, and Wakabayashi K. Beta-catenin is frequently mutated and demonstrates altered cellular location in azoxymethane-induced rat colon tumors. Cancer Res. **58**: 42–46. 1998. [Medline]
32. Takahashi M, Mutoh M, Kawamori T, Sugimura T, and Wakabayashi K. Altered expression of beta-catenin, inducible nitric oxide synthase and cyclooxygenase-2 in azoxymethane-induced rat colon carcinogenesis. Carcinogenesis. **21**: 1319–1327. 2000. [Medline] [CrossRef]